Journal of Materials Chemistry B

Accepted Manuscript

ROYAL SOCIETY OF CHEMISTRY

www.rsc.org/materialsB

Journal Name

ARTICLE

Thermo and pH Dual-Controlled Charge Reversal Amphiphilic Graft Copolymer Micelles for Overcoming Drug Resistance in Cancer Cells

Received 00th January 20xx,
Accepted 00th January 20xx

DOI: 10.1039/x0xx00000x

www.rsc.org/

Haitao Zhang,[a] Xiao-dong Fan,[a,] † Fei Li,[b] Rongtian Suo,[a] Hui Li, [a] Zhen Yang,[a] Wanbin Zhang,[a] Yang Bai,[c] Wei Tian,[a,]†

Currently, multidrug resistance (MDR) is the major challenge of nanotechnology in cancer treatment. In this study, a series of amphiphilic poly(styrene-*co*-maleic anhydride)-*graft*-poly(2-(*N*,*N*-dimethylamino)ethyl methacrylate) graft copolymer [$PSMA_{89}$-g-P(DMA_{16}-co-SD)] micelles, was prepared. $PSMA_{89}$-g-P(DMA_{16}-co-SD) graft copolymers were first synthesized by grafting different amounts of sulfadimethoxine (SD) onto $PSMA_{89}$-g-P(DMA_{16}-co-SD). The $PSMA_{89}$-g-P(DMA_{16}-co-SD_{56}) micelles exhibited a thermo and pH dual-controlled charge reversal property without cleavage of chemical bonds. The surface charge of $PSMA_{89}$-g-P(DMA_{16}-co-SD_{56}) micelles reversed from positive to negative after the solution temperature increased from 25 °C to 37 °C at pH 7.4. However, when the pH value was adjusted to 6.8 at 37 °C, the surface charge became positive again. The thermo and pH dual-controlled charge reversal not only resulted in a controlled doxorubicin (DOX) release but also effectively enhanced the cellular uptake of DOX-loaded $PSMA_{89}$-*g*-P(DMA_{16}-*co*-SD_{56}) micelles through electrostatic absorptive endocytosis. MTT assay demonstrated that DOX-loaded $PSMA_{89}$-*g*-P(DMA_{16}-*co*-SD_{56}) micelles showed the highest inhibition growth of DOX-resistant ovarian carcinoma (A2780/Dox^R) cells with pH 6.8 at 37 °C among those with pH 7.4 at 37 °C and pH 7.4 at 25 °C, leading to higher efficiency in overcoming MDR of A2780/Dox^R cells. Therefore, $PSMA_{89}$-*g*-P(DMA_{16}-*co*-SD_{56}) micelles can be used as intelligent drug-delivery systems to overcome MDR of cancercells.

1. Introduction

Multidrug resistance (MDR) is a major challenge to the effective treatment of cancer.[1–3] MDR cancer cells have shown limited capacity to defend themselves against cytotoxic chemicals.[4] Thus, realizing a sufficiently high intracellular level of cytotoxic chemicals by using an optimized delivery system may represent a novel tactic to overcome MDR of cancer cells. Nanoscale vehicles as drug carriers provide an alternative strategy to circumvent MDR by offering a way to encapsulate or attach drugs to nanomaterials, such as lipids, polymers, and solid-core nanoparticles, which are resistant to drug efflux mediated by permeability glycoprotein (P-gp).[5,6] Among these nanomaterials, pH-triggered charge reversal nanoparticles have been widely designed to facilitate tumor cell uptake and enhance inhibition of cancer cells.[7–9] An ideal nanocarrier should be negatively charged or uncharged in the physiological environment to reduce toxicity and prolong blood circulation time, whereas the activated cationic charges in tumor tissues and their intracellular compartments promote the cellular uptake, as well as assist the endosomal escape. For example, Wang et al. reported that dual pH-sensitive nanoparticles of a polymer-DOX conjugate (PPC-Hyd-DOX-DA) can reverse the surface charge from negative to positive at pH 6.8 by acid-responsive cleavage of β-carboxyl amide bonds, thereby facilitating tumor cell internalization and DOX release at endosomal pH because of hydrazone cleavage.[10]These dual pH-responsive DOX prodrug nanoparticles demonstrated enhanced inhibition of drug-resistant SK-3rd cancer stem cells.[11] However, to date, majority of reversely charged nanoparticles are single pH-responsive, and the reversible processof surfaces charge cannot be completely conducted without the cleavage of β-carboxyl amide bonds.[12, 13] Additionally, the preparation process was complicated. Therefore, double- or multi-stimuli-responsive charge reversal micelles without the cleavage of the chemical bonds for drug resistance in cancer cells should be explored.

Alternatively, the emergence of pH and thermo dual-responsive drug carriers self-assembled from amphiphilic copolymers has introduced a new generation of anticancer

[a] *The Key Laboratory of Space Applied Physics and Chemistry, Ministry of Education and Shaanxi Key Laboratory of Macromolecular Science and Technology, School of Science, Northwestern Polytechnical University, Xi'an, 710072, P. R. China Address here.*
[b] *Department of Pharmacy, 456 Hospital of People's Liberation Army, Ji'nan 250000, China*
[c] *Xi'an Modern chemistry Research Institute, Xi'an, 710065, P. R. China*
† Corresponding author. E-mail: happytw_3000@nwpu.edu.cn (W.T.), xfand@126.com (X.F.)
Electronic Supplementary Information (ESI) available: Synthesis of hydroxyl -poly(N, N-dimethylaminoethyl methacrylate) (HO-PDMA), Dz, LCST and ztea potential change of DOX loaded $PSMA_{89}$-g-P(DMA_{16}-co-SD_{56}) micelles. See DOI: 10.1039/x0xx00000x

drug-delivery systems that are more intelligent and more effective than the conventional ones.[14–19] Enhancing drug-loading capability and controlling the lower critical solution temperature (LCST) of polymeric systems above the body temperature (37 °C) are the major challenges for the thermo and pH dual-responsive drug carriers. Compared with amphiphilic block copolymers, amphiphilic graft copolymers can easily form micelles because of several polymer chains, and the properties of the micelles can be more easily varied by simply adjusting the graft frequency and length of the branches.[20–23] Moreover, the graft copolymer micelles exhibit higher drug-loading capacity and entrapment efficiency than those of the block copolymer micelles.[24] Therefore, the development of amphiphilic graft copolymer micelles with temperature and pH dual-controlled charge reverse and higher LCST (>37 °C) at physiological environment will represent a promising drug-delivery system to overcome drug resistance in cancer cells.

Considering the information above, we intend to construct amphiphilic graft copolymer-based charge reverse micelles by using sulfadimethoxine (SD), poly(2-(dimethylamino) ethyl methacrylate) (PDMA), and poly-styrene-maleic anhydride copolymer (PSMA) as building blocks. From the viewpoint of functional structure design, sulfonamide derivatives show weak negatively charged properties because of the ionization of sulfonamide group (SO_2NH) in aqueous media.[25] Among these building blocks, SD has been widely used in pH-responsive biomedical materials (e.g., cancer-targeted drug carrier systems) [26,27] because of its pKa of about 6.2, which is close to the physiological pH, tumor extracellular region (pH 7.2 to 6.5), and intracellular endosomal environment (pH 5 to 6).[28,29]PDMA is a widely studied thermo-responsive cationic polymer that has been used in conjugation with hyperthermia treatment for localized drug delivery at tumor sites.[30–36] PSMA-based prodrugs and functional nanoparticleshave also been widely reported.[37–41] More importantly, partial ammonolysis of anhydride with ammonia results in an amide and a carboxylic acid group (so-called amic acid),[42] which can stabilize and negatively charge SMA-based particles in aqueous medium through electrostatic interactions and ionization of carboxylic acid group, respectively.

In the present study, we prepared a thermo and pH dual-controlled charge reversal micelle based on SD-modified amphiphilic graft copolymers to overcome drug resistance in cancer cells. A series of amphiphilic graft copolymers, $PSMA_{89}$-*g*-P(DMA_{16}-*co*-SD_{13}), $PSMA_{89}$-*g*-P(DMA_{16}-*co*-SD_{31}) and $PSMA_{89}$-*g*-P(DMA_{16}-*co*-SD_{56}), bearing different amounts of SD units and a certain amount of PDMA chains grafted on the backbone of PSMA were first synthesized by esterification and amidation reaction. These amphiphilic graft copolymers can self-assemble into core-shell-structured micelles in aqueous solution, which presented pH and thermo dual-responsive properties. Particularly, $PSMA_{89}$-*g*-P(DMA_{16}-*co*-SD_{56}) micelles were positively charged at 25 °C and pH 7.4. However, as the temperature increased to 37 °C at pH 7.4, the micelles became negatively charged. The surface charge of the $PSMA_{89}$-g-P(DMA_{16}-co-SD_{56}) micelles was expected to reverse from negative to positive when the pH decreased from pH 7.4 to pH 6.8 at 37 °C. The reverse characteristics of surface charge of $PSMA_{89}$-g-P(DMA_{16}-co-SD_{56}) micelles can enhance uptake efficiency and the MDR ability when they arrived at the cancer tissues (Scheme 1).

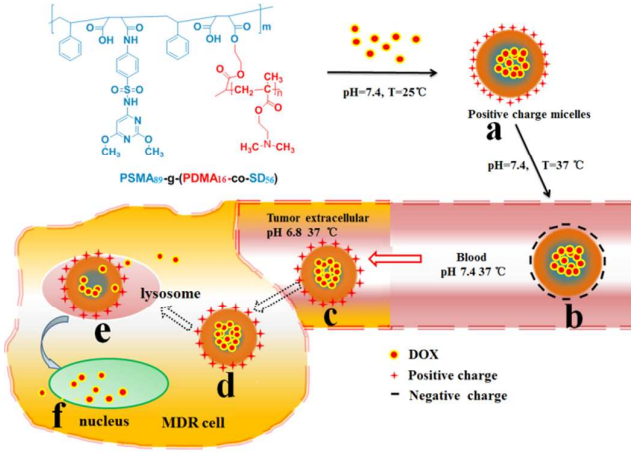

Scheme 1. Possible mechanism of charge reversal and cell uptake mechanism for $PSMA_{89}$-g-P(DMA_{16}-co-SD_{56})/DOX micelles. (a) DOX-loaded $PSMA_{89}$-g-P(DMA_{16}-co-SD_{56}) micelles with positive charge at 25 °C and pH 7.4; (a-b) the micelles were negatively charged in blood circulation; (b-c) negative surface charge of the micelles was reversed to positive after the micelles reached the tumors; (c-d) uptake efficiency was enhanced; and (d-f) DOX molecules were released from the micelles in the cells to overcome drug resistance.

2. Results and Discussion

2.1 Synthesis of PSMA-*g*-P(DMA-*co*-SD)

PSMA-g-P(DMA-co-SD) was synthesized by grafting hydroxyl-poly-PDMA (HO-PDMA)and the different amounts of SD onto PSMA through ammonolysis and esterolysis (Scheme 2 and Table 1). PSMA with degree of polymerization of 89 and a polydispersity of 1.32 was first prepared through radical copolymerization of maleic anhydride (MA) and styrene (St)corresponding to the reference.[43] HO-PDMA,with degree of polymerization of 16 and a polydispersity of 1.24 determined by SEC-MALLS(Fig. S3), was synthesized by atom transfer radical polymerization(ATRP) of DMA monomer with 2-hydroxyethyl-2-chloropropanoate (HECP) as the initiator (Supporting information, SI; Figs. S1 and S2)

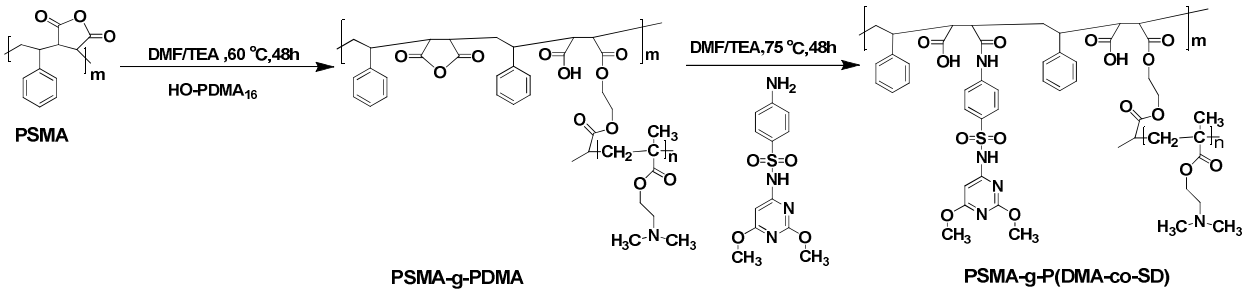

Scheme 2. Synthesis routes of PSMA-g-P(DMA-co-SD) graft copolymers.

The polymer structure of PSMA-*g*-P(DMA-*co*-SD) was further confirmed through proton nuclear magnetic resonance (^{1}H NMR), Fourier transform infrared spectroscopy (FTIR), and size exclusion chromatography-multi-angle laser light scattering (SEC-MALLS). Fig. 1 shows the ^{1}H NMR spectra of $PSMA_{89}$ (Fig. 1A), $PSMA_{89}$-*g*-$PDMA_{16}$ (Fig. 1B), and $PSMA_{89}$-*g*-P(DMA_{16}-*co*-SD_{56}) (Fig. 1C). Compared with the ^{1}H NMR spectra of $PSMA_{89}$-*g*-$PDMA_{16}$ and PSMA, signals associated with SD (peaks p, q, and r) and PDMA (peaks l and h) were clearly found, and the proton peak signal of the new chemical group acylamino (NHCO) was at 9.53 ppm (peak m'). Furthermore, the coverage degree of PDMA segments can be calculated by the integral ratio of the phenyl protons (7.26 ppm) of St and the methylene protons (1.75 ppm). The coverage degree of PDMA was 16%, and the integral ratio of the sulfonamide group (SO_2NH, 11.25 ppm) of the phenyl protons of St units (7.26 ppm) was used to calculate the coverage degrees of SD. The coverage degrees of SD in $PSMA_{89}$-g-P(DMA_{16}-co-SD_{13}), $PSMA_{89}$-g-P(DMA_{16}-co-SD_{31}), and $PSMA_{89}$-g-P(DMA_{16}-co-SD_{56}) were 13%, 30%, and 56%, respectively (Table 1). Figs. 1D–1F show the FTIR spectra for $PSMA_{89}$, $PSMA_{89}$-g-$PDMA_{16}$, and $PSMA_{89}$-g-P(DMA_{16}-co-SD_{56}). Some evident differences can be observed by comparing the spectra of $PSMA_{89}$-g-P(DMA_{16}-co-SD_{56}) with those of $PSMA_{89}$ and $PSMA_{89}$-g-$PDMA_{16}$. First, the stretching vibration of O-H bond in the carboxylic acid groups and N-H bond in the groups merged as a broad band at 3424 cm^{-1}. Second, absorption peaks at 1858 and 1778 cm^{-1} related to the stretching vibration of C=O of MA units decreased significantly, whereas the bands at 1730 and 1649 cm^{-1} corresponding to ester (ν_C= O) and amide (ν_C= O) groups appeared and separated well. Moreover, a shoulder peak of C=O band of the carboxylic acid groups was observed at 1710 cm^{-1}. The SEC-MALLS results of graft copolymers are listed in Table 1. PSMA-*g*-P(DMA-*co*-SD) exhibited a higher M_w value than $PSMA_{89}$ and $PSMA_{89}$-g-$PDMA_{16}$. Furthermore, the M_w values of a series of PSMA-*g*-P(DMA-*co*-SD) increased from 51500 to 61800 with the increase of coverage degrees of SD from 13% to 56%. The ^{1}H NMR, FTIR, and SEC-MALLS results indicated that HO-PDMA segments and SD units were successfully grafted to the side chain of PSMA.

Table 1. Molecular structure parameters of resulting polymers

Polymers	Degree of coverage[a] (%)	*Degree of COOH*[b]	M_w[c]	M_n[d]	PDI[e]
PSMA	-		18000	13100	1.37
$PSMA_{89}$-g-$PDMA_{16}$	16	16	46200	35100	1.32
$PSMA_{89}$-g-P(DMA_{13}-co-SD_{13})	13	26	51500	38700	1.33
$PSMA_{89}$-g-P(DMA_{13}-co-SD_{30})	30	43	56400	43100	1.31
$PSMA_{89}$-g-P(DMA_{13}-co-SD_{56})	56	69	61800	48600	1.27

[a]The coverage degrees of PDMA and SD were calculated by the integral ratio of ^{1}H NMR;[b]The coverage degrees of COOH were equal to the total the coverage degrees of SD and HO-PDMA;[c,d]The weight-average molecular weight (Mw) and number-average molecular weight (Mn) were determined by SEC-MALLS;[e]Polydispersity index was determined by SEC-MALLS.

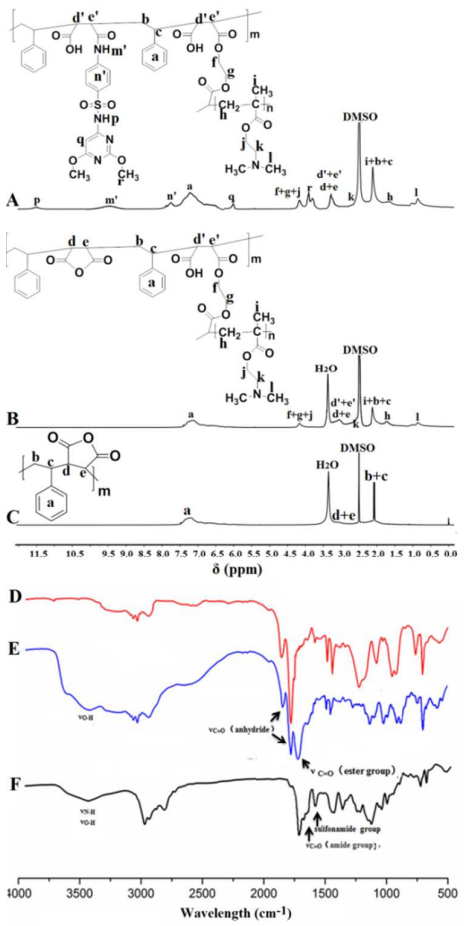

Fig. 1. ^{1}H NMR spectra of $PSMA_{89}$-g-P(DMA_{16}-co-SD_{56}) (A), $PSMA_{89}$-g-$PDMA_{16}$ (B), and $PSMA_{89}$ (C) (DMSO-d_6, 298 K); FTIR spectra of $PSMA_{89}$ (D), $PSMA_{89}$-g-$PDMA_{16}$ (E), and $PSMA_{89}$-g-P(DMA_{16}-co-SD_{56}) (F).

2.2 Thermo and pH Dual-Responsive $PSMA_{89}$-g-P(DMA_{16}-co-SD) Micelles

A series of amphiphilic graft copolymers $PSMA_{89}$-g-P(DMA_{16}-co-SD) was prepared on the basis of the above results. Their self-assembly was easily promoted by directly dissolving $PSMA_{89}$-g-P(DMA_{16}-co-SD) in water with a concentration of 0.5 mg/mL at 25 °C. Fluorescence spectrophotometry (FL), ^{1}H NMR [in deuterium oxide (D_2O)], transmission electron microscopy (TEM), and dynamic light scattering (DLS) measurements were conducted to obtain further insights into theself-assembly of these graft copolymer micelles.

Critical micelle concentration (CMC) is one of the most physicochemical parameters of the micellization behavior of amphiphilic copolymers in diluted aqueous solution.[44] The CMC of $PSMA_{89}$-g-P(DMA_{16}-co-SD) was determined through the fluorescence technique with pyrene as a probe (Fig. 2Aand Table 2). The coverage degree of SD in $PSMA_{89}$-g-P(DMA_{16}-co-SD) increased from 0 to 56 and induced the remarkable decrease of CMC values from 7.2 μg/mL to 3.6 μg/mL. These results may be attributed to the introduction of SD that increased the hydrophobicity and reduced the repulsion between backbone polymer chains.[45] The ^{1}H NMR spectra of $PSMA_{89}$-g-P(DMA_{16}-co-SD_{56}) in DMSO-d_6 exhibited the chemical shifts of the PSMA backbone, PDMA, and SD side chains (Fig. 2B-a). However, the only proton peaks of methoxyl and methylene protons of PDMA moieties were observed in the medium of D_2O (Fig. 2B-b). These results demonstrated that $PSMA_{89}$-*g*-P(DMA_{16}-*co*-SD_{56}) self-assembled into micelles consisting of hydrophobic PSMA and SD inner core surrounded by a hydrophilic PDMA outer shell in aqueous solution.

Table 2. Physicochemical parameters of $PSMA_{89}$-g-P(DMA_{16}-co-SD) micelles in aqueous solution (0.5 mg/mL)

Micelles	CMC[a] (μg/ml)	D_{av}[b] (nm)	D_z[c] (nm)	PDI[d]	Zeta potential (mV)[e]		LCST[f](°C)
					pH=7.4	pH=6.8	
$PSMA_{89}$-g-$PDMA_{16}$	7.5	78	93	0.172	8.8	31.5	33.5
$PSMA_{89}$-g-P(DMA_{16}-co-SD_{13})	5.8	133	167	0.213	8.2	30.2	35.7
$PSMA_{89}$-g-P(DMA_{16}-co-SD_{30})	4.9	156	182	0.206	7.8	28.4	36.9
$PSMA_{89}$-g-P(DMA_{16}-co-SD_{56})	3.6	175	204	0.217	4.3	26.2	38.3

[a] Determined by a fluorescence spectroscopic method with pyrene as fluorescence probe at 25 °C;[b] Average diameter determined by TEM; [c] Z-average diameter determined by DLS; [d] Polydispersity of particles diameter determined by DLS; [e] Determined by DLS at 25°C;[f] LCST values determined by turbidity measurements.

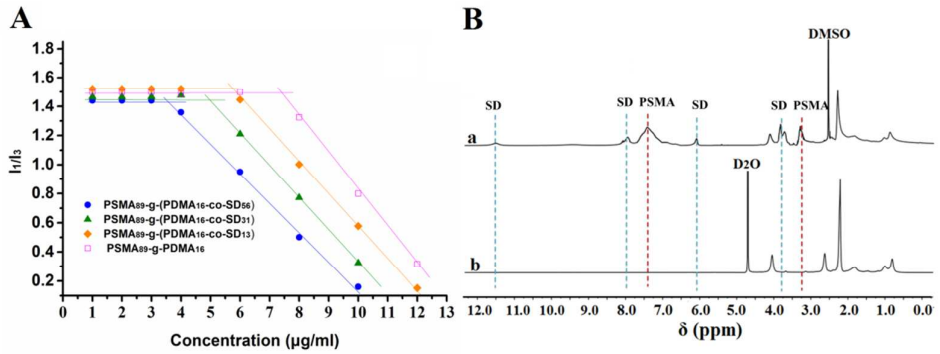

Fig. 2. Plot of I_1/I_3 in the excitation spectra versus the concentrations of all graft copolymers (A); ^{1}H NMR spectra of PSMA$_{89}$-*g*-P(DMA$_{16}$-*co*-SD$_{56}$) micelles in dimethyl sulfoxide (DMSO) (B-a) and in deuterated oxide (D_2O) (B-b), respectively.

Furthermore, DLS and TEM measurements were used to evaluate the size and morphology of PSMA$_{89}$-*g*-P(DMA$_{16}$-*co*-SD) micelles. DLS measurements showed that PSMA$_{89}$-*g*-P(DMA$_{16}$-*co*-SD) self-assembled into micelles with a Z-average diameter (D_z) ranging from 167 nm to 204 nm and a low polydispersity index (PDI < 0.25) (Fig. 3A and Table 2). The sizes of the PSMA$_{89}$-*g*-P(DMA$_{16}$-*co*-SD) micelles were larger than those of the PSMA$_{89}$-*g*-PDMA$_{16}$ micelles and also increased with the increase of SD content. Alternatively, TEM was used to observe the morphology of the PSMA$_{89}$-*g*-P(DMA$_{16}$-*co*-SD) micelles. With careful staining of the micelles using 2 wt% phosphotungstic acid, the core-shell structure was clearly revealed where SD and PSMA appeared as bright areas and PDMA lied in the darker regions circling the cores independent of the core-shell proportion. This further revealed that PSMA$_{89}$-*g*-P(DMA$_{16}$-*co*-SD) could form core-shell-structured micelles in aqueous solution (Fig. 3B). The average diameter (D_{av}) of PSMA$_{89}$-*g*-P(DMA$_{16}$-*co*-SD) micelles increased from 133 nm to 175 nm with the increase of SD content (Fig. 3B and Table 2), which was in accordance with the DLS results. This increase in size upon increasing hydrophobic block ratio in graft copolymer was observed for another amphiphilic graft copolymer system.[46]

Thermo and pH dual-responsive properties of PSMA$_{89}$-g-P(DMA$_{16}$-co-SD) micelles were carefully investigated. LCST is an important parameter for studying thermo-responsive drug-delivery systems.[47] The LCST values of micelles in different pH buffer solutions were determined by monitoring the optical transmittance change as a function of temperature. The LCSTs of PSMA$_{89}$-*g*-P(DMA$_{16}$-*co*-SD) micelles were all higher than those of PSMA$_{89}$-PDMA$_{16}$ micelles at pH 7.4 (Fig. 4A and Table 2), whereas the LCST behavior of micelles disappeared at pH 6.8 (Fig. 4B). A reasonable explanation indicates that PDMA becomes a typical non-thermo-sensitive polymer at neutral condition because tertiary amine groups are protonated and positively charged.[48]Additionally, the LCST value of the micelles increased from 35.7 °C to 38.3 °C as the coverage degree of SD increased from 13 to 56 at pH 7.4. TEM and DLS were used to further prove the thermo and pH-responsive property. As shown in Figure S4, PSMA$_{89}$-*g*-P(DMA$_{16}$-*co*-SD$_{56}$) micelles still hold a core-shell morphology at 37°C and at pH 6.8.Therefore, PSMA$_{89}$-*g*-P(DMA$_{16}$-*co*-SD$_{56}$) micelles were selected for further research based on a lower CMC of 3.6 μg/ml and higher LCST of 38.3 °C; moreover, PSMA$_{89}$-*g*-P(DMA$_{16}$-*co*-SD$_{56}$) can self-assemble into stable core-shell micelles at body temperature and inhibited drug leakage conditions.[49]

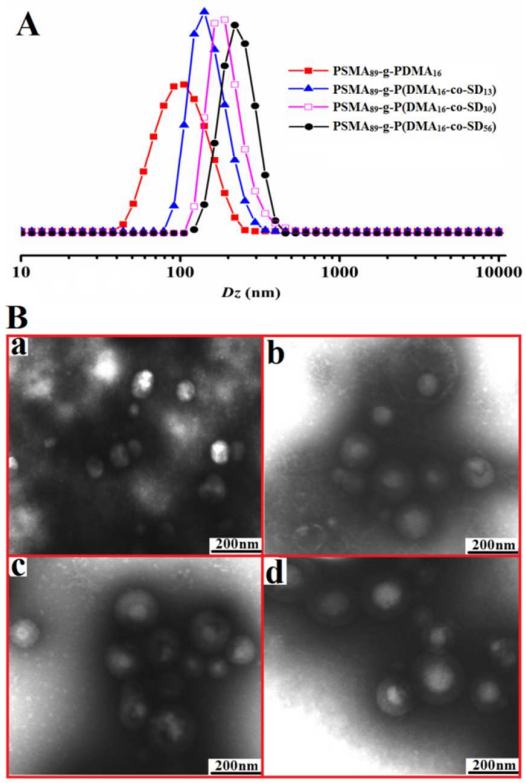

Fig. 3. (A) Typical intensity-averaged diameter distributions of all graft copolymer aqueous solutions at 0.5 mg/mL, 25 °C and pH 7.4; (B) TEM images of all graft copolymers micelles with 2% phosphotungstic acid at 25 °C and pH 7.4. (a: PSMA$_{89}$-g-PDMA$_{16}$; b: PSMA$_{89}$-g-P(DMA$_{16}$-co-SD$_{13}$); c: PSMA$_{89}$-g-P(DMA$_{16}$-co-SD$_{30}$); d: PSMA$_{89}$-g-P(DMA$_{16}$-co-SD$_{56}$).

2.3 Thermo and pH Dual-Controlled Charge Reversal Property of PSMA$_{89}$-*g*-P(DMA$_{16}$-*co*-SD$_{56}$) Micelles

To overcome drug resistance in cancer cells, thermo and pH dual-controlled charge reversal properties of PSMA$_{89}$-g-P(DMA$_{16}$-co-SD$_{56}$) micelles were investigated. As shown in Fig. 5, the zeta potential of PSMA$_{89}$-g-P(DMA$_{16}$-co-SD$_{56}$) micelles decreased from +4.3 mV to −6.2 mV as temperature increased from 25 °C to 37 °C at pH 7.4 (Figs. 5a-b), whereas the zeta potential quickly increased from −6.2 mV to +22.3 mV after the pH value was adjusted from 7.4 to 6.8 at 37 °C (Figs. 5 b-c). The zeta potential then increased to +25.2 mV as the temperature decreased to 25 °C at pH 6.8 (Fig. 5 c-d). Generally, the tumor extracellular environment is slightly acidic (pHe = 6.8) and the pH of the bloodstream is approximately 7.4. Thus, the above results indicated that PSMA$_{89}$-*g*-P(DMA$_{16}$-*co*-SD$_{56}$) micelles will be negatively charged in the blood circulation (zeta potential is −6.2 mV at pH 7.4 and 37 °C in Fig. 5), which will minimize the undesirable rapid elimination of PSMA$_{89}$-*g*-P(DMA$_{16}$-*co*-SD$_{56}$) micelles from the blood circulation and facilitate their accumulation at the tumor sites.[50] Furthermore, the surface charge of PSMA$_{89}$-*g*-P(DMA$_{16}$-*co*-SD$_{56}$) micelles will change to positive in the tumor extracellular fluid (zeta potential is +4.2 mV at pH 6.8 in Fig. 5), which will enhance the uptake of PSMA$_{89}$-*g*-P(DMA$_{16}$-*co*-SD$_{56}$) micelles. Moreover, PSMA$_{89}$-g-P(DMA$_{16}$-co-SD$_{13}$) and PSMA$_{89}$-g-P(DMA$_{16}$-co-SD$_{31}$) micelles had the similar zeta potential trend (Figure S5). But their LCST were all lower than 37 °C at pH 7.4 (Figure 4A), leading to drug leakage before the micelles got the lesions.[49] Therefore, only PSMA$_{89}$-*g*-P(DMA$_{16}$-*co*-SD$_{56}$) micelles demonstrate an excellent potential for thermo and pH-triggered charge reversal drug delivery in tumors.

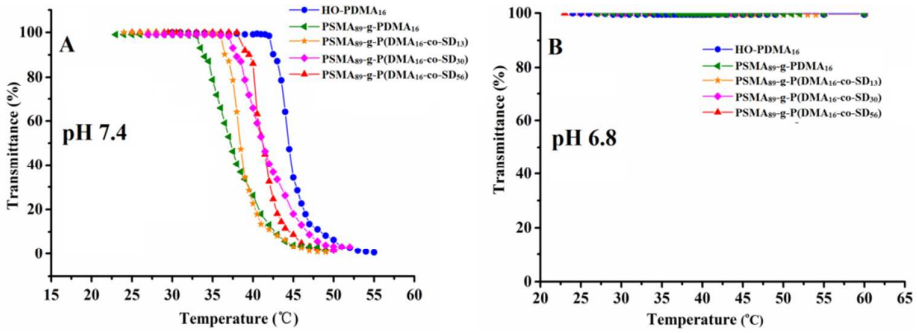

Fig. 4. Optical transmittance of all graft copolymers aqueous solutions with a concentration of 0.5 mg/mL in phosphate-buffer saline. (A) pH 6.8; (B) 7.4.

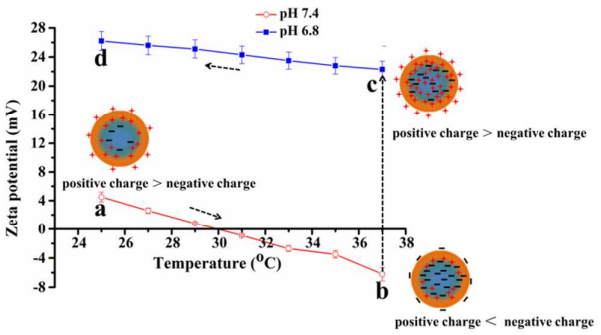

Fig. 5. Zeta potential value of PSMA$_{89}$-g-P(DMA$_{16}$-co-SD$_{56}$) micelles as a function of solution temperature. (a-b) temperature increased from 25 °Cto 37 °C at pH 7.4; (b-c) pH was adjusted from 7.4 to 6.8 at 37 °C; (c-d) temperature decreased to 25 °C at pH 6.8.

The mechanism for the above thermo and pH dual-controlled charge reversal property was further proposed. From the viewpoint of molecular structure, partial ammonolysis and esterification of the anhydride in PSMA generated the amount of -COOH groups. It has been reported SD and -COOH groups can carry anion charges through part ionization (Eqs. 1 and 2) which could result in the nanoparticle surface was negative-charged.[51,25] In addition, PSMA$_{89}$-*g*-P(DMA$_{16}$-*co*-SD$_{56}$) micelles had two pKa values induced by the existence of SD and –COOH (Figure S6A). The pKa of PSMA$_{89}$-*g*-P(DMA$_{16}$-*co*-SD$_{56}$) micelles decreased with the increase of temperature (Figure S6B), leading the enhanced degree of ionization of SD and –COOH.[52] Therefore, the amount of negative charge of PSMA$_{89}$-*g*-P(DMA$_{16}$-*co*-SD$_{56}$) micelles surface increased with the increase of temperature. Finally, the amount of negative charge was higher than positive charge on the surface of PSMA$_{89}$-*g*-P(DMA$_{16}$-*co*-SD$_{56}$) micelles, leading to the surface charge of PSMA$_{89}$-*g*-P(DMA$_{16}$-*co*-SD$_{56}$) micelles reversed from positive to negative in Figure 5 (a-b). Similar temperature influence on pKa and zeta potential has been reported in previous literature.[53,54] On the other aspect, the tertiary amine groups of PDMA segments were all protonated at pH 6.8 and generated numerous positive charges on the surfaces of PSMA$_{89}$-*g*-P(DMA$_{16}$-*co*-SD$_{56}$) micelles.[48] Meanwhile, SD and –COOH changed from ionized form to deionized form and the degree of ionization of SD and COOH decreased when the pH value was adjusted to 6.8, leading to the decrease of negative charge. Therefore, the number of positive charge was higher than that of negative charge in PSMA$_{89}$-*g*-P(DMA$_{16}$-*co*-SD$_{56}$) micelles. Thus, the PSMA$_{89}$-*g*-P(DMA$_{16}$-*co*-SD$_{56}$) micelles were positively charged again after the pH value was adjusted to 6.8 at 37 °C (Figure 5 b-c).

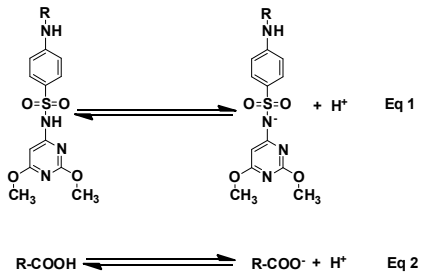

2.4 In Vitro Release, Cellular Uptake, and Distribution of $PSMA_{89}$-g-$P(DMA_{16}$-co-$SD_{56})$/DOX Micelles

The anticancer drug doxorubicin (DOX) was used to study the temperature and pH-induced controlled release from $PSMA_{89}$-g-$P(DMA_{16}$-co-$SD_{56})$ micelles because of its fluorescence properties. The physical entrapment of DOX into $PSMA_{89}$-g-$P(DMA_{16}$-co-$SD_{56})$ micelles was achieved through a dialysis technique. To obtain a high amount of DOX incorporation, triethylamine was added to remove hydrochloride from DOX·HCl. The loading content and loading efficiency were 10.6% and 67.4%, respectively. DOX loading slightly increased the size of $PSMA_{89}$-*g*-$P(DMA_{16}$-*co*-$SD_{56})$ to an average diameter of 223 nm (Fig. S7), whereas the LCST and zeta potential values of DOX-loaded $PSMA_{89}$-g-$P(DMA_{16}$-co-$SD_{56})$ micelles did not change compared with unloaded $PSMA_{89}$-g-$P(DMA_{16}$-co-$SD_{56})$ micelles (Fig. S8). Fig. 6 shows the release of DOX from $PSMA_{89}$-*g*-$P(DMA_{16}$-*co*-$SD_{56})$ micelles at temperatures above and below the LCST with pH 7.4 and 6.8 PBS solutions. Apparently, the in vitro release showed certain thermo and pH sensitivities. The release rate and cumulative release amount of DOX from $PSMA_{89}$-g-$P(DMA_{16}$-co-$SD_{56})$ micelles were faster and higher at pH 6.8 than that those at pH 7.4. The protonated and positively charged tertiary amine groups from PDMA segments may contribute to the different release behaviors at pH 6.8. Moreover, DOX is an amphoteric drug containing protonable amino group and deprotonable phenolic groups; thus, DOX was protonated and positively charged in acidic media.[55]The increased electrostatic repulsion force between DOX and PDMA was ascribed to the faster drug release from $PSMA_{89}$-*g*-$P(DMA_{16}$-*co*-$SD_{56})$ micelles at pH 6.8 than that at pH 7.4.[56] Moreover, a high temperature was found helpful for drug release. For instance, 8.9% and 15.3% DOX amounts were released from $PSMA_{89}$-*g*-$P(DMA_{16}$-*co*-$SD_{56})$ micelles after 30 h at 25 °C and 37 °C, respectively. More negative charges in the core produced by the enhanced degree of ionization of sulfonyl group in SD and COOH made the hydrophobic core become more mobile at high temperature.[57] Thus, drug movement within the polymer matrix became easier.

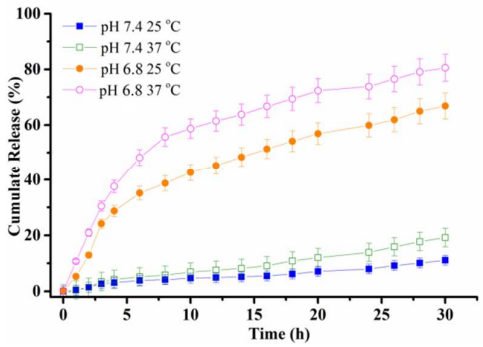

Fig. 6. Release of DOX from $PSMA_{89}$-g-$P(DMA_{16}$-co-$SD_{56})$ at pH 7.4, 25 °C; pH 7.4, 37 °C; and pH 6.8, 25 °C; pH 6.8, 37 °C.

To demonstrate the effect of charge reversibility of $PSMA_{89}$-g-$P(DMA_{16}$-co-$SD_{56})$ micelles on the cellular internalization process, the cell uptake of free DOX and DOX-loaded $PSMA_{89}$-g-$P(DMA_{16}$-co-$SD_{56})$ micelles at pH 7.4 and 6.8 were investigated on A2780/Dox^R cells through fluorescence microscopy. Fig. 7 shows the A2780/Dox^R cell uptake efficiency of $PSMA_{89}$-g-$P(DMA_{16}$-co-$SD_{56})$/DOX micelles and free DOX at 1.0, 2.0, 4.0, and 6.0 h cell cultures. Up to 2 μg/mL equivalent DOX concentration in the culture medium was applied. Noticeably, $PSMA_{89}$-g-$P(DMA_{16}$-co-$SD_{56})$/DOX micelles demonstrated much higher cellular uptake efficiency than the free drug. Generally, micelles are more effectively internalized into cells through an endocytosis procedure rather than passive diffusion of the free drug. Even negatively charged particles can be internalized by cells through caveolae-mediated endocytosis despite the unfavorable interaction between the particles and the negatively charged plasma membrane.[58,59] Only the drug present in the cell membrane can be refluxed out of the cancer cell by P-gp. Therefore, the DOX uptake efficiency in A2780/DoxR cells treated with $PSMA_{89}$-g-$P(DMA_{16}$-co-$SD_{56})$/DOX micelles at pH 7.4 and 6.8 was much higher than in those treated with free DOX. Moreover, at 37 °C, the cellular uptake efficiency at pH 6.8 was higher than that at pH 7.4. This result can be ascribed to the occurrence of electrostatic attraction between micelles and the cell membrane because of the charge reversal from negative to positive as a consequence of pronated PDMA at acidic pH, thus enhancing the cellular internalization. Although the positive charge was higher at pH 6.8 than that at pH 7.4 at room temperature, no significant cellular uptake efficiency difference was observed in the cellular uptake at pH 6.8 at 37 °C and pH 7.4 at 25 °C. These results indicated that the amount of positive charges and temperature did notsignificantly influence the cellular uptake efficiency of $PSMA_{89}$-g-$P(DMA_{16}$-co-$SD_{56})$/DOX micelles.

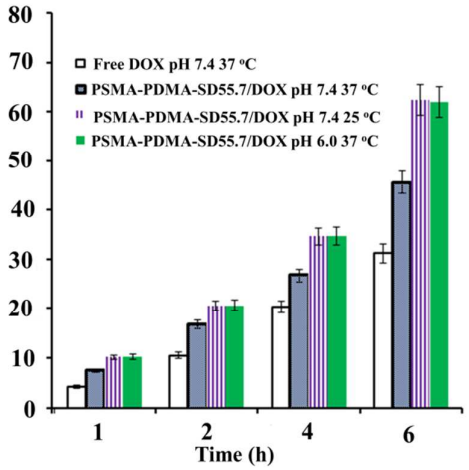

Fig. 7. A2780/Dox^R cell uptake efficiency of free DOX at pH 7.4, 37 °C, and PSMA$_{89}$-g-P(DMA$_{16}$-co-SD$_{56}$)/DOX at pH 7.4, 25 °C; pH 7.4, 37 °C and pH 6.8, 37 °C. (n = 6, p < 0.05).

To further investigate the effect of the cellular internalization process, the cell uptake was investigated using fluorescence microscopy. DOX showed an intrinsic red fluorescence, and cell nucleus stained with Hoechst33342 showed a blue fluorescence. The merged images displayed the overlay of red fluorescence of DOX and blue Hoechst33342 staining of nuclei. The cells exposed to free DOX exhibited a noticeable fluorescence signal in the nucleus (evidenced by purple dots in nucleus, a sign of colocalization of DOX with Hoechst33342) and a relatively weak fluorescence signal in the cytoplasm (evidenced by red dots of DOX signal) (Fig. 8A). This observation can be explained by the cellular uptake mechanism of free DOX, which was basically through passive diffusion, and A2780/Dox^R cells that produced drug resistance to DOX. Fluorescence microscopy images of A2780/DOX^R cells incubated with PSMA$_{89}$-g-P(DMA$_{16}$-co-SD$_{56}$)/DOX micelles at 25 °C and 37 °C at pH 7.4 are shown in Figs. 8B and 8C. Noticeably, DOX fluorescence intensity in the tumor cells at 25 °C was much higher than that at 37 °C because of the charge reversal from positive to negative as temperature increased from 25 °C to 37 °C, thus weakening the cellular internalization. Moreover, the cells treated at 37 °C and pH 6.8 showed almost similar fluorescence intensity in the cytoplasm compared with the cells treated at 25 °C and pH 7.4. However, much broad red fluorescence distribution in the nucleus was found at 37 °C and pH 6.8 (Fig. 8D). These phenomena can be explained as follows: 1) PSMA$_{89}$-g-P(DMA$_{16}$-co-SD$_{56}$)/DOX micelles were positively charged at both experiment conditions, and the cell uptake efficiency of PSMA$_{89}$-g-P(DMA$_{16}$-co-SD$_{56}$)/DOX was equal (Fig. 7). 2) At pH 6.8, the DOX release rate was faster at 37 °C than that at 25 °C (Fig. 7). More free DOX amounts were released from PSMA$_{89}$-g-P(DMA$_{16}$-co-SD$_{56}$)/DOX micelles even at a certain amount of PSMA$_{89}$-g-P(DMA$_{16}$-co-SD$_{56}$)/DOX micelles. Therefore, more DOX amounts entered the nucleus and much broader red fluorescence distribution was found at 37 °C and pH 6.8. These results demonstrated that temperature and pH triggered charge reversal micelles for intracellular drug delivery and can significantly enhance cellular uptake, leading to a high efficacy of overcoming MDR.

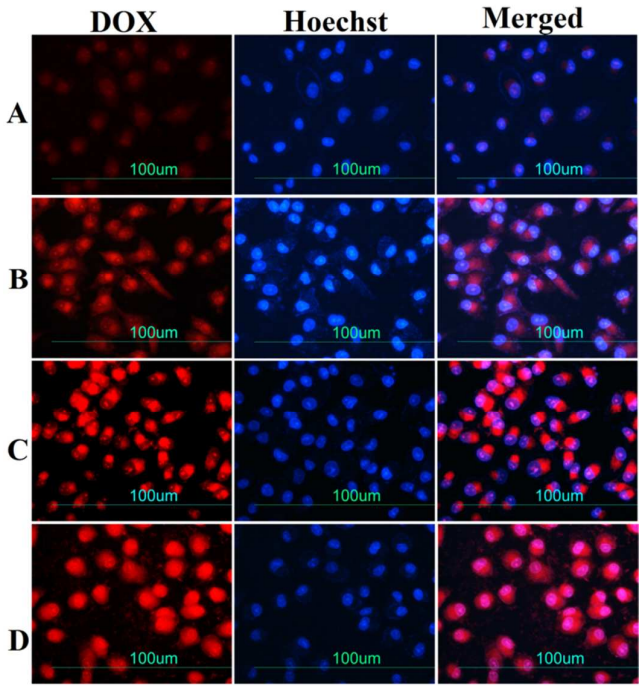

Fig. 8 Confocal microcopy studies of cellular uptake and controlled release behaviors of DOX (pH 7.4, 37 °C) (A) and PSMA$_{89}$-g-P(DMA$_{16}$-co-SD$_{56}$)/DOX micelles (at pH 7.4, 37 °C (B); pH 7.4, 25 °C; (C) and pH 6.8, 37 °C) after incubation with A2780/Dox^R cells for 12 h at a concentration of 0.5 μg /mL.

2.5 Cell Viability Assays of PSMA$_{89}$-g-P(DMA$_{16}$-co-SD$_{56}$) Micelles

The in vitro biocompatibility and cytotoxicity of PSMA$_{89}$-g-P(DMA$_{16}$-co-SD$_{56}$) micelles toward A2780/Dox^R cells were evaluated using MTT assay. The viability of cells treated with PSMA$_{89}$-g-P(DMA$_{16}$-co-SD$_{56}$) micelles for 24 h was evaluated at all test concentrations up to 120 μg/mL (Fig. 9A). The PSMA$_{89}$-g-P(DMA$_{16}$-co-SD$_{56}$) polymer has been demonstrated as biocompatible and nontoxic, which indicated that PSMA$_{89}$-g-P(DMA$_{16}$-co-SD$_{56}$) can be safely used as biocompatible carriers for efficient intracellular drug delivery. The viability of A2780/Dox^R cells after incubation with free DOX and PSMA-g-P(DMA-co-SD$_{56}$)/DOX micelles was evaluated (Fig. 9B). All the studied cell lines showed a typical dose–response sigmoidal curve. The in vitro half maximal inhibitory concentration (IC$_{50}$) values of PSMA$_{89}$-g-P(DMA$_{16}$-co-SD$_{56}$)/DOX micelles were 0.81 and 3.8 μg/mL at pH 6.8 and 7.4, respectively, whereas the IC$_{50}$ was 11.6 μg/mL for free DOX. Compared with free DOX, PSMA-g-P(DMA-co-SD$_{56}$)/DOX micelles exhibited enhanced growth inhibition effects on A2780/Dox^R cells and overcame the MDR of A2780/Dox^R cells. This phenomenon was also observed by Wang et al. on tumor acidity-activated charge conversional, DOX-loaded PAMA-DMMA nanogels.[60] This result can be attributed to the positively charged PSMA$_{89}$-g-P(DMA$_{16}$-co-SD$_{56}$)/DOX micelles at pH 6.8, which

were more readily internalized by cells than the negative $PSMA_{89}$-g-P(DMA_{16}-co-SD_{56})/DOX micelles at pH 7.4. However, no significant cellular uptake efficiency difference was observed at 25 °C at pH 7.4 and 37 °C at pH 6.8 (Fig. 7). The IC_{50} of $PSMA_{89}$-g-P(DMA_{16}-co-SD_{56})/DOX micelles also showed lower growth inhibition effects on A2780/Dox^R cells at 25 °C than that at 37 °C, which was mostly attributable to the accelerated drug release in acidic intracellular compartments with the increase of temperature.

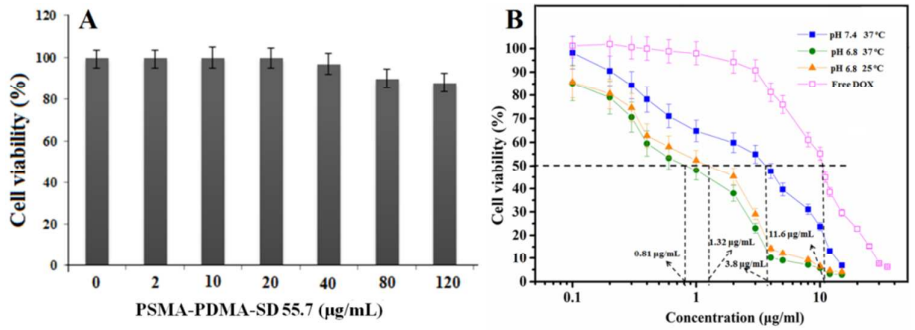

Fig. 9. (A) In vitro cytotoxicity of plain $PSMA_{89}$-g-P(DMA_{16}-co-SD_{56}) micelle; (B) $PSMA_{89}$-g-P(DMA_{16}-co-SD_{56})/DOX micelles (at pH 6.8 and 37 °C, pH 6.8 and 25 °C, pH 7.4 and 37 °C) and free DOX (pH 7.4 and 37 °C) against A2780/DOX^R cancer cell line.

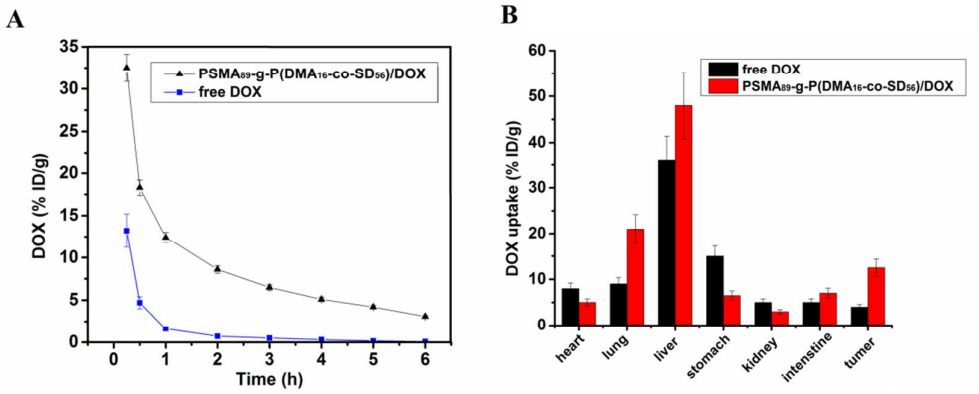

Fig.10. (A) Pharmacodynamic behavior of $PSMA_{89}$-g-P(DMA_{16}-co-SD_{56})/DOX and DOX studied by measuring their blood circulation in mice with fluorescence spectroscopy. Concentrations of DOX in blood were measured at various time points after tail vein injection with $PSMA_{89}$-g-P(DMA_{16}-co-SD_{56})/DOX and free DOX (5 mg/kg of DOX concentration); (B) Biodistribution of DOX and $PSMA_{89}$-g-P(DMA_{16}-co-SD_{56})/DOX in major organs at 6 h after tail vein injection (5 mg/kg of DOX concentration) into nude mice bearing A2780 tumor. The values plotted are mean ± SD of five experiments.

2.6 Pharmacokinetics and biodistribution of $PSMA_{89}$-g-P(DMA_{16}-co-SD_{56}) Micelles

To investigate the in vivo pharmacokinetics and biodistribution, $PSMA_{89}$-g-P(DMA_{16}-co-SD_{56})/DOX micelles and free DOX were injected into mice through the tail vein, respectively. As shown in Fig. 10A, $PSMA_{89}$-g-P(DMA_{16}-co-SD_{56})/DOX micelles showed a prolonged half-time in blood circulation, as compared with the free DOX. The DOX circulation half-time increased from 0.5 h for free DOX to 2 h for $PSMA_{89}$-g-P(DMA_{16}-co-SD_{56})/DOX micelles. As shown in Fig. 10B, $PSMA_{89}$-g-P(DMA_{16}-co-SD_{56})/DOX micelles exhibited a higher tumor uptake but lower uptake to all normal organs including liver and lungthan that of free DOX. Generally, compare to positive-charged nanocarries, negative-charged nanocarries shown a higher potential protein resistance and longer circulation for in vivo experiments.[60] In contrast, cell membranes arenegatively charged, positively charged nanocarriers shown a higher affinity for cell membrane and are expected to be internalizedmore efficiently than those negatively charged.[61] Moreover, as discovered in Figure 5, $PSMA_{89}$-g-P(DMA_{16}-co-SD_{56})/DOX micelles surface was negative-charged in normal physiological environment, and was positive-charged after getting the tumor tissue. Thus, $PSMA_{89}$-g-P(DMA_{16}-co-SD_{56})/DOX micelles exhibited a higher tumor uptake than that of free DOX. The above results confirmed that $PSMA_{89}$-g-P(DMA_{16}-co-SD_{56})/DOX micelles with the function of thermo- and pH-controlled charge reversal and can efficiently load and deliver DOX into tumor cells, which are highly promising as efficient nanocarriers to overcome MDR.

3. Conclusions

A series of thermo and pH dual-responsive $PSMA_{89}$-g-P(DMA_{16}-co-SD) graft copolymer micelles with fixed content of PDMA and different amounts of SD was conveniently prepared. The content of SD influenced the size, CMC, LCST, and zeta potential of these micelles. The enhanced degree of ionization of SD and COOH groups induced the zeta potential of $PSMA_{89}$-g-P(DMA_{16}-co-SD_{56}) micelles to reverse from positive charges to negative ones at pH 7.4 and 37 °C, whereas the protonated PDMA segments drove the zeta potential to reverse into positive again at pH 6.8 and 37 °C. DOX-loaded $PSMA_{89}$-*g*-P(DMA_{16}-*co*-SD_{56}) micelles showed pH- and thermo-controlled drug release behavior.Cellular uptake efficiency and fluorescence microscopy observations indicated that more DOX was delivered into the cytoplasm of A2780/Dox^R cells treated with DOX-loaded $PSMA_{89}$-g-P(DMA_{16}-co-SD_{56}) micelle at 25 °C and pH 7.4 than that at 37 °C and pH 7.4. Moreover, no significant cellular uptake efficiency difference was observed in the cellular uptake at pH 6.8 and 37 °C and at pH 7.4 and 25 °C. However, fluorescence microscopy observations probed that more DOX was delivered into the nucleus of A2780/Dox^R cells at pH 6.8 and 37 °C. MTT assays revealed that the thermo and pH dual-controlled charge reversal enhanced the efficiency of DOX-loaded $PSMA_{89}$-*g*-P(DMA_{16}-*co*-SD_{56}) micelles to overcome the MDR of A2780/Dox^R cells at pH 6.8 and 37 °C. The DOX-loaded $PSMA_{89}$-*g*-P(DMA_{16}-*co*-SD_{56}) micelles showed a longer circulation time and higher tumer uptake than free DOX. Therefore, $PSMA_{89}$-*g*-P(DMA_{16}-*co*-SD_{56}) micelles exhibit great potential as drug-delivery carriers to overcome MDR.

4. Experimental Section

4.1 Materials: 2,2′-Azobis-(isobutyronitrile) (AIBN), St, MA were purchased from Aldrich. MA was recrystallized in chloroform before use. CuCl, Ethylene glycol, *2,2′*-bipyridyne (bpy), 2-Chloropropionyl chloride, *N, N*-dimethylaminoethyl methacrylate (DMA), SD, and doxorubicin hydrochloride (DOX·HCl) were purchased from Aldrich. Methylene chloride, anhydrous magnesium sulfate, copper chloride ($CuCl_2$), DMF, 2-butanone, tetrahydrofuran (THF), diethyl ether, TEA, methanol, and dimethyl sulfoxide (DMSO) were from Shanghai Sinopharm Chemical Reagent Co., Ltd. 3-(4,5-dimethylthiazol-2-yl)-2,5-diphenyl tetrazolium bromide (MTT), Dulbecco's modified eagle medium (DMEM), Trypsin-EDTA, and Hoechst33342 were obtained from Sigma Chemical Co. (USA). Dimethyl formamide (DMF) and dimethylsulfoxide (DMSO) were obtained from Baotelai Chemicals (Xi'an, China).

4.2 Methods

^{1}H NMR spectroscopy was performed on a Bruker-Avance III NMR spectrometer (400 MHz) with deuterated chloroform ($CDCl_3$), D_2O, and deuterated dimethyl sulfoxide (DMSO-d_6) as solvents. Fourier transform infrared (FT-IR) spectra were recorded on a PerkinElmer Paragon 1000 spectrometer through the KBr sample holder method. Spectra were obtained by collecting and averaging 16 scans at frequencies ranging from 500 cm^{-1} to 4000 cm^{-1} at room temperature. The molecular structure parameters of the resulting polymers were determined on a DAWN EOS SEC/MALLS instrument equipped with a viscometer (Wyatt Technology, USA). High-performance liquid chromatography (HPLC)-grade DMF containing LiCl (0.01 mol/L) (at 45 °C) was used as eluent at a flow rate of 0.5 mL/min. The emission spectra were recorded by FL (Hitachi F-4600, Japan) from 350 nm to 470 nm with an excitation wavelength of 335 nm. Particle size was measured by Zetasizer Nano-ZS dynamic light scattering (DLS) (Malvern Instruments, UK). TEM measurements were performed on JEM-2010 microscope (Japan) with an electron kinetic energy of 300 keV. TEM samples were prepared in an oven at constant temperatures of 25 °C and 37 °C. To observe the nanoparticles, a drop of the nanoparticle dispersion was performed. The sample was pre-thermostated at 25 °C then deposited onto a carbon-coated copper EM grid and exposed to phosphotungstic acid for 10 min before measurement.

4.3 Synthesis of Poly(styrene-*co*-maleic anhydride)-*graft*-Poly(2-(*N,N*-dimethylamino-co- Sulfadimethoxine)

4.3.1 Synthesis of Hydroxyl-poly[*2-(N,N-dimethylamino* methacrylate)]

HO-PDMA with M_w = 2100 was prepared via ATRP of DMA monomer with HECP as the initiator and CuBr/bpy as catalysts (Scheme 2). The detailed preparation progress is presented in the Supporting Information (SI).

4.3.2 Synthesis of Poly(styrene-*co*-maleic anhydride)

Approximately 4.91 g of MA (0.05 mol) was dissolved in 100 mL of methyl ethyl ketone in a 150 mL glass flask and 5.25 g of St (99%, 0.05 mol) was added. The solution was deoxygenated with nitrogen, and 0.11 g of AIBN (6.7 × 10^{-4}mol) was added. The polymerization was performed at 70 °C for 7 h. The polymer product was precipitated in 500 mL diethyl ether and dried in a vacuum. The structure and molecular weight ofpoly(styrene-*co*-maleic anhydride) (PSMA)were determined by ^{1}H NMR, FTIR, and SEC-MALLS. The experimental values are as follows: ^{1}H NMR (DMSO$_{-d6}$): 7.60-6.00 (br, pH H), 3.33 (s, H_2O), 3.60-2.80 [br, CH=CH (MAh unit)], 2.80-1.50 [br, CH_3-DMSO and CH_2-CH (St unit)]. IR (KBr, cm^{-1}): 3033, 2929, 1858, 1778, 1561, 1492, 1451, 1326, 1224, 1085, 954, 917, 759, 700. SEC-MALLS(DMF as eluent): M_n = 14800 (DP = 53); M_w/M_n = 1.37.

4.3.3 Synthesis of Poly(styrene-co-maleic anhydride)-graft-Poly(2-(N,N-dimethylamino)ethyl methacrylate

The reaction was performed with DMF as the solvent in a degassed flask. The procedure was conducted as follows. First, 0.42 g (0.02 mmol) HO-PDMA, 4.47 mg (0.04 mmol) TEA, and 2.02 g (0.1 mmol) PSMA were dissolved in DMF. After the solution was thoroughly deoxygenated by three freeze-pump-thaw cycles, the tube was sealed and heated to 60 °C for 48 h. After being cooled to room temperature, the obtained DMF solution was slowly dropped into about 40 mL of THF, the precipitate was collected and purified by

reprecipitation from methanol/THF. The obtained white precipitate was recovered by filtration and characterized by the combined techniques of ^{1}H NMR, and SEC-MALLS. The experimental values are as follows: ^{1}H NMR (DMSO-*d6*): 7.60-6.00 (br, Ph H), 3.33 [s, H_2O), 3.60-2.80 (br, CH-CH (MAh unit)], 2.80-1.50 [br, CH_3-DMSO and CH_2-CH (St unit)], 3.99 (m O-CH_2), 2.50 (br, CH_3-DMSO and N-CH_2), 2.20 (m N-CH_3), 1.75 (s -CH_2-), 0.96 (C-CH_3). M_w/M_n = 1.32.

4.3.4 Synthesis of Poly(styrene-*co*-maleic anhydride)-*graft*-Poly(2-(*N,N*-dimethylamino-co-Sulfadimethoxine)

Double TEA and 0.031 g (0. 1 mmol), 0.062 g (0.2 mol), and 0.124g (0.8 mol) of SD and were dissolved in DMF. Then the solution was added to a DMF solution of 0.46 mg (0.1 mmol) PSMA-g-PDMA inside a Schlenk tube. After the solution was thoroughly deoxygenated by three freeze-pump-thaw cycles, the tube was sealed and heated to 75 °C for 48 h. After being cooled to room temperature, the obtained DMF solution was slowly dropped into excessive THF, the precipitate was collected and purified by reprecipitation from methanol/THF(2/1,v/v).The obtained white precipitate was recovered through filtration and characterized by the combined techniques of ^{1}H NMR and SEC-MALLS. The experimental values were as follows: ^{1}H NMR (DMSO-*d6*): 11.45 (SO_2NH), 9.33 (s, NHCO), 7.82 and 7.60-6.00 (br, Ph H), 3.72 (s, O-CH_3), 3.33 (s, H_2O), 3.60-2.80 [br, CH-CH (MAh unit)], 2.80-1.50 [br, CH_3-DMSO and CH_2-CH (St unit)], 3.99 (m, O-CH_2), 2.50 (br, CH_3-DMSO and N-CH_2), 2.20(m, N-CH_3), 1.75 (s, -CH_2-), 0.96 (s, CH_3).

4.4 Self-Assembly of $PSMA_{89}$-g-P(DMA_{16}-co-SD)and Critical Micelles Concentrations (CMCs) Determination

$PSMA_{89}$-g-P(DMA_{16}-co-SD)graft copolymers micelles were prepared through a dialysis method. Briefly, 5.0 mg of $PSMA_{89}$-g-P(DMA_{16}-co-SD) graft copolymer was dissolved in 2 mL of DMF, and then 8 mL of distilled water was slowly added to the stirring solution. Stirring was continued for another 10 h, and the solution was then dialyzed against distilled water for 2 d, during which the distilled water was replaced every 6 h.

CMCs of the copolymers were estimated through a fluorescence spectroscopic method using pyrene as the fluorescence probe at 25 °C. Typically, pyrene solutions in acetone were added to each brown bottle. Acetone was then evaporated, leaving 1.0×10^{-6}mol of pyrene in each bottle. Aqueous solutions (10 mL) of $PSMA_{89}$-g-P(DMA_{16}-co-SD)graft copolymers at concentrations ranging from 0.15 g/L to 0.005 g/L were added to the bottles. The mixtures were stirred at 25 °C for 20 h and sonicated for 1 min before measurement.

4.5 Thermo- and pH-sensitivity of $PSMA_{89}$-g-P(DMA_{16}-co-SD) micelles

The LCST of $PSMA_{89}$-g-P(DMA_{16}-co-SD) was determined by the cloud point method. Briefly, the optical transmittance of the copolymer aqueous solution (1 mg/mL) at pH 7.4 and 6.8 was measured against temperature by UV-vis spectroscopy (Shimadzu UV-2560 model spectroscopy, Shimadzu, Japan) at a wavelength of 560 nm. The temperature of the sample cells increased with a rate of 0.5 °C/min from 20 °C to 60 °C.

The size and Zeta potential of $PSMA_{89}$-g-P(DMA_{16}-co-SD)micelles were measured by dynamic light scattering (DLS), through a Malvern Instrument Zetasizer Nano ZS with a scattering angle of 1738 and 633 nm red laser at different temperatures and pH. The aqueous solution of $PSMA_{89}$-g-P(DMA_{16}-co-SD) micelles was added into the sample cell thermosstated at the given temperatures and pH for 3 min prior to measurement.

4.6 Drug loading and in *vitro* Release of Thermo and pH-responsive micelles

An anticancer drug DOX was encapsulated into $PSMA_{89}$-g-P(DMA_{16}-co-SD) micelles through a simple dialysis technique. Briefly, DOX·HCl (3.0 mg) and threefold molar TEA were dissolved in DMSO (4 mL) and continuously stirred for 4 h to remove hydrochloride. After this, 8 mg graft copolymer was added to form a homogeneous solution. Distilled water (20 mL) was added into the solution through a syringe to form polymeric micelles after stirring for 5 h. This solution was dialyzed against distilled water for 24 h to remove the residual DMSO and untapped DOX. After dialysis, the loading amount of DOX in nanoparticles was determined by dissolving 5 mL freeze-dried solution into 25 mL DMSO before UV-vis measurements. The concentration of DOX was calculated according to the standard curve of the DOX-PBS solution. Drug loading content (DLC) and drug loading efficiency (DLE) were calculated using the following equations:

$$\mathrm{DLC}(\%) = \frac{\text{weight of loaded drug}}{\text{weight of drug} - \text{loaded micelles}} \times 100\%$$

$$\mathrm{DLE}(\%) = \frac{\text{weight of loaded drug}}{\text{weight of drug in feed}} \times 100\%$$

In vitro drug release profiles were obtained using a dynamic dialysis method. The release experiments were conducted at 25 °C and 37 °C. Typically, a micelle solution of 200 μg/mL equivalent DOX concentration was placed into a dialysis bag and introduced to 100 mL of phosphate buffered saline (PBS; 0.1 mol/L, pH = 6.8, 7.4) with magnetic stirring at 200 rpm. At hourly intervals, 3 mL samples were removed from the release medium, and the same volume and temperature of fresh PBS was added to the release medium. The accumulated drug release of DOX was determined using UV-vis measurements.

4.7 Cell Culture

The DOX-resistant ovarian carcinoma A2780 (A2780/Dox^R) cell line (provided kindly by the Department of Gynecology and Obstetrics, Xijing Hospital Xi'an, China) were used as in vitro models. The cells were cultured in DMEM supplemented with fetal bovine serum (FBS) (final concentration 10% v/v) and antibiotics. The cells were cultured at 37 °C at 5% CO_2 humidified atmosphere. The cells were harvested with 0.02%

(w/v) EDTA-0.025% (w/v) trypsin and rinsed. The resulting cell suspension was used in the following experiments.

4.8 Cellular Uptake Study

A2780/Dox^R cells were seeded in 12-well plate at a density of 2×10^5 cells/well. When the cells reached about 80% confluence, the medium was replaced by 1.0 mL DOX, and DOX-loaded PSMA-g-P(DMA-co-SD)$_3$ micellar solutions with a DOX concentration of 2 μg/mL at different pH (6.0, 7.4) without serum. These solutions were incubated in a humidified incubator with 5% CO_2 atmosphere at 37 °C for 1 h. Subsequently, the medium was discarded, and the cells were washed thrice with PBS (pH 7.4). Cells were then detached by 0.02% (w/v) EDTA-0.025% (w/v) trypsin solution, spun down through centrifugation and dispersed again in 0.5 mL of PBS for flow cytometric measurements. Nanocarrier uptake was analyzed based on the DOX fluorescence through a flow cytometer (BD FACSAria).

4.9 In Vitro Cytotoxicity Assay against Cancer Cells

MTT cell proliferation assay was used to evaluate thecytotoxicity of plain PSMA$_{89}$-g-P(DMA$_{16}$-co-SD) micelles and DOX-loaded PSMA$_{89}$-g-P(DMA$_{16}$-co-SD) nanoparticles. A2780/Dox^R cancer cells were seeded onto 96-well culture plates (5×10^3 cells per well) and cultured for 24 h. The original media (200 μL) were removed and replaced with plain PSMA$_{89}$-g-P(DMA$_{16}$-co-SD) micellar solutions with a concentration range of 2 μg/mL to 120 μg/mL, or DOX-loaded PSMA$_{89}$-g-PDMA$_{16}$-SD micellar solutions with a DOX concentration range of 0.05 μg/mL to 40 μg/mL, and were then allowed to incubate for 48 h. Simultaneously, free DOX was used as the control. Afterward, 20 μL of MTT reagent (5 μg/mL) was added to each well and incubated for 4 h. The culture medium was removed, and 150 uL DMSO was added. The plate was shaken for 20s, and the absorbance was immediately measured at 570 nm using an ELX800 absorbance microplate reader (Bio-Tek EPOCH, Winooski, VT, USA). The cytotoxicity was expressed as a percentage of the control, and the IC_{50} value was determined as the DOX concentration required to reduce the absorbance to 50% in the untreated control wells.

4.10 Pharmacokinetics and biodistribution of PSMA$_{89}$-g-P(DMA$_{16}$-co-SD$_{56}$) Micelles

4.10.1 *In vivo* pharmacokinetic study

PSMA$_{89}$-g-P(DMA$_{16}$-co-SD$_{56}$) /DOX micelles and Free DOX in PBS equivalent to 5 mg/kg DOX was administered to Balb/c mice by tail vein injection, respectively. DOX measurement was according to the previously reported protocols with minor modifications.[62] After predetermined time intervals, approximately 20 mL of blood was drawn from the tail vein of U87 MG tumor bearing nude mice to measure the bloodcirculation of DOX. Briefly, the blood samples were dissolved in lysis buffer 1(defined by 1% sodium dodecylsulfate (SDS), 1% Triton X-100, 40 m Mtris(hydroxymethyl)aminomethane (tris) acetate, 10 mM ethylene diamine tetra-acetic acid (EDTA), and 10 m Mdithiothreitol (DTT). Then DOX was extracted by incubating blood samples in 1 mL HCl (0.75 N) in isopropanol at 20 °C overnight. Aftercentrifugation at 15,000 rpm for 20 min, the fluorescence of the supernatant was measured using a fluorescence spectrophotometry (LS-55 fluorescence spectrophotometer, PerkineElmer, USA).

4.10.2 Biodistribution study

Nude mice bearing A2780 tumors were sacrificed at 30 min and 6 h after tail vein injection with PSMA$_{89}$-g-P(DMA$_{16}$-co-SD$_{56}$) /DOX micelles and free DOX in PBS at a concentration of 5 mg/kg DOX. The organs/tissues (0.1-0.3 g wet-weight of each) were homogenizedin 0.5 mL of lysis buffer 2 (defined by 0.25 M sucrose, 40mM tris-acetate, 10mMEDTA). For DOX concentrations detection, 200 mL of each tissue lysates was mixed with 100 mL of 10% Titron X-100. After strong vortexing, DOX was extracted byadding the samples into 1 mL of the extraction solution (0.75 N HCl in isopropanol) and then incubating at 20 °C overnight. Then after centrifugation at 15,000 rpm for 20 min, the fluorescence of the supernatant was measured.

4.11 Statistics

Statistical analysis was conducted by using the Student's t-test with $p < 0.05$ as significant difference.

Acknowledgements

We gratefully thank the financial support of National Science Foundations of China (No. 21274116 and No. 21374088). W.T. thanks the grant from the Program for New Century Excellent Talents of Ministry of Education (NCET-13-0476), the Key Laboratory Program of Science and Technology Coordinator Innovation Project of Shaanxi Province of China (2013SZS17-P01), the Program of New Staff and Research Area Project of NPU (13GH014602).

Notes and references

1 M. Kavallaris, *Nat. Rev. Cancer,* 2010, **10**, 194-204.
2 G. Tian, X. P. Zheng, X. Zhang, W. A. Yin, J.Yu, D. L. Wang, Z. P. Zhang, X. L. Yang, Z. J. Gu and Y. L. Zhang, *Biomaterials,* 2015, **40**, 107-116.
3 P. Savage, J. Stebbing, M. Bower and T. Crook,*Nat.Clin.Pract. Oncol.,*2009, **6**, 43-52.
4 D.Kim, E. S. Lee, K. T. Oh, Z. G. Gao and Y. H. Bae,*Small,*2008, **4**, 2043-2050.
5 X. W.Dong and R. J. Mumper, *Nanomedicine,* 2010, **5**, 597-615.
6 Y. C. Wang, F. Wang, T. M. Sun and J. Wang, *Bioconjugate Chem.,*2011,**22**, 1939-1945.
7 H. Z. Deng, J. J. Liu, X. F. Zhao, Y. M. Zhang, J. F. Liu, S. X. Xu,L. D. Deng, A. J. Dong and J. H. Zhang, *Biomacromolecules,*2014, **15**, 4281-4292.
8 Y. Huang, Z. H. Tang, X. F. Zhang, H. Y. Yu, H. Sun, X. Pang andX. S. Chen, *Biomacromolecules,* 2013, **14**, 2023-2032.

9 T. Zhou, X. M. Zhou and D.Xing, *Biomaterials,*2014, **35**, 4185-4194.
10 J. Z. Du, X. J. Du, C. Q. Mao and J.Wang, *J. Am. Chem. Soc.,*2011, **133**, 17560-17563..
11 F. H. Meng, Y. A. Zhong, R. Cheng, C. Deng and Z. Y.Zhong, *Nanomedicine,*2014,**9**, 487-499.
12 P. Xu, E. A. Van Kirk, Y. H. Zhan, W. J. Murdoch, M.Radosz and Y. Q.Shen,*Angew. Chem., Int.Ed.,*2007, **46**, 4999-5002.
13 G. F. Luo, W. H. Chen, Y. Liu, Q. Lei, R. X.Zhuo and X. Z. Zhang,*Sci. Rep.,* 2014,**4**, 6064.
14 M. Duvvuri and J.P. Krise, *Front.Biosci.,*2005, **10**, 1499-14509.
15 S.Zhao, S. W. Tan, Y. Y.Guo, J. H Huang, M. C. Chu, H. D. Liu and Z. P. Zhang,*Biomacromolecules,*2013, **14**, 2636-2646.
16 Q. J. He, Y. Gao, L. X. Zhang, Z. W. Zhang, F. Gao, X. F.Ji, Y. P. Li and J. L.Shi, *Biomaterials,* 2011, **32**, 7711-7720.
17 Y. Li, F. Wang, T. M. Sun, J. Z. Du, X. Z. Yang and J. Wang, *Sci. China Chem.,* 2014, **57**, 579-585.
18 T. Stover, Y. Kim, T. Lowe and M. Kester, *Biomaterials,* 2008, **29**, 359-369.
19 S.Kapse-Mistry, T. Govender, R. Srivastava and M. Yergeri,*Front.Pharmacol.,*2014, **5**,159.
20 V. Gemma, T. P. Judit and F. Fernando,*Curr. Drug Deliv.,*2012,**9**, 367-394.
21 M. G. McKee, S. Unal, G. L. Wilkes and T. E. Long,*Prog.Polym. Sci.,*2005,**30**, 507-539.
22 X. J. Zhang, F. J. Chen, Z. L. Zhong and R. X. Zhuo,*Macromol. Rapid.Commun.,*2010,**31**, 2155-2159.
23 G. Riess,*Prog.Polym. Sci.,* 2003, **28**, 1107-1170.
24 V. Torchilin, *Adv. Drug Deliv. Rev.,* 2011, **63**, 131-135.
25 S. I. Kang and Y. H. Bae,*J.Controlled Release,*2002, **80**, 145-155.
26 S. Bersani, M.Vila-Caballer, C. Brazzale, M. Barattin, and S. Salmaso,*Eur. J. Pharm.Biopharm.,*2014, **88**, 670-682.
27 V. A. Sethuraman, K. Na and Y, H. Bae,*Biomacromolecules,*2006,**7**, 64-70.
28 K. Ulbrich and V.Subr,*Adv. Drug.Deliv. Rev.,* 2004, **56**, 1023-1050.
29 G. R. Martin and R. K.Jain, *Cancer Res*., 1994, **54**, 5670-5674.
30 M. Nakayama and T. Okano,*Macromolecules,*2008, **41**, 504-507.
31 X. Han, X. X. Zhang, H. F. Zhu, Q. Y. Yin, H. L. Liu and Y. Hu,*Langmuir,*2013,**29**, 1024-1034.
32 K. Y. Sui, X. Zhao, Z. M. Wu, Y. Z. Xia, H. C. Liang and Y. J. Li,*Langmuir*, 2012,**28**, 153-160.
33 Y. L. Luo, X. J. Yao, J. F. Yuan, T. Ding and Q. Y. Gao,*Colloids Surf. B,*2009,**68**, 218-224.
34 R. Iwai, Y. Nemoto and Y. Nakayama,*Biomaterials,* 2013,**34**, 9096-9102.
35 S. T.Guo, Y. Y. Huang, W. D. Zhang, W. W. Wang, T. Wei, D. S. Lin,J. F. Xing, L. D. Deng, Q. Du, Z. C. Liang, X. J. Liang and A. J. Dong, *Biomaterials,* 2011,**32**, 4283-4292.
36 S. Venkataraman, W. L. Ong, Z. Y. Ong, S. C.JoachimLoo, P. L. Ee and Y. Y. Yang,*Biomaterials,* 2011, **32**, 2369-2378.
37 X. P.Duan, J. S. Xiao, Q. Yin, Z. W. Zhang, H. J. Yu, S. R. Mao and Y. P.Li, *ACS Nano*, 2013,**7**, 5858-5869.
38 K.Greish, T. Sawa, J. Fang, T. Akaike and H.Maeda, *J. Controlled Release,*2004,**97**, 219-230.
39 Z. Wang, M. Gao, J. Sun, D. H. Liang and X.Jia, *Macromolecules,* 2013,**46**, 1723-1731.
40 S. M.Henry, M. E. El-Sayed, C. M. Pirie, A. S. Hoffman and P. S. Stayton,*Biomacromolecules,* 2006,**7**, 2407-2414.
41 C. L. Yi, N. Liu, J. C. Zheng, J. Q. Jiang and X. Y.Liu,*J. Colloid Interface Sci.* 2012, **380**, 90-98.
42 W. J. Soer, W. H. Ming, L. Klumperman, C. E. Koning and R. van Benthem,*Polymer,* 2006, **47**, 7621-7627.
43 X. C. Yin and H. D. H.Stöever, *Macromolecules,* 2002, **35**, 10178-10181.
44 C. L. Lo, S. J. Lin, H. C. Tsai, W. H. Chan, C. H. Tsai, C. H. Cheng and G. H. Hsiue,*Biomaterials,* 2009, **30**, 3961-3970.
45 J. Lu and M. S. Shoichet, *Macromolecules,* 2010,**43**, 4943-4953.
46 R. S. Lee and Y. T. Huang,*Polym. J.,* 2010,**42**, 304-312.
47 R. Cheng, F. H.Meng, C. Deng, H. A. Klok and Z. Y. Zhong,*Biomaterials,* 2013, **34**, 3647-3657.
48 X. Han, X. X. Zhang, Q. Y. Yin, H. L. Liu and Y. Hu, *Macromol. Rapid.Commun.,* 2013, **34**, 574-580
49 G. F. Chen, R. Y. Chen, C. X. Zou, D. W. Yang and Z. S. Chen, *J. Mater. Chem. B,*2014,**2**, 1327-1334.
50 Z. X. Zhou, Y. Q. Shen, J. B. Tang, E. L. Jin, X. P. Ma, Q. H. Sun, B. Zhang, E. A. Van Kirk, W. J. Murdoch, *J. Mater. Chem.,*2011,**21**, 19114-19123.
51 O. C.Farokhzad, S. Jon, A.Khademhosseini, T. N. Tran, D. A.Lavan and R. Langer. *Cancer Res.* 2004, **64**, 7668-7672.
52 T. Radeva, Physical Chemistry of Polyelectrolytes. CRC Press, 2001, ch 17, PP. 654-659.
53 P.Mpofu, J.Addai-Mensah, J. Ralston.*J. Colloid. Interface Sci.* 2004,**271**, 145-56.
54 A. Clausen, T. Dowling, and G. Bicker, *J. Liq.Chrom. & Rel. Technol.* 2002, **25**, 705-715.
55 C. Sanson. C. Schatz, J. F. Le Meins, A. Soum, J. Thévenot, E. Garanger, S.Lecommandoux,*J. Controlled Release,* 2010, **147**, 428-435.
56 Y. Tian, L. Bromberg, S. N. Lin, T. A. Hatton and K. C.Tam, *J. Controlled Release,* 2007, **121**, 137-145.
57 L. Y. Zhang, R. Guo, M. Yang, X. Q. Jiang and B. R.Liu,*Adv. Mater.,*2007, **19**, 2988-2992.
58 G. Sahay, D. Y. Alakhova and A. V. Kabanov,*J. Controlled Release,*2010,**145**, 182-195.
59 Q. Mu, G. Jiang, L. Chen, H. Zhou, D. Fourches, A. Tropsha and B.Yan,*Chem. Rev.,*2014,**114**, 7740-7781.
60 J. Z.Du, T. M. Sun, W. J. Song, J. Wu, J.Wang,*Angew. Chem., Int.Ed.,*2010, **49**, 3621-3626.
61 V.Mailander, K.Landfester, *Biomacromolecules*, 2009, **10**, 2379–2400.
62 Y. K. Lee, J. Choi, W. Wang, S.Lee, T. H. Nam, W. S. Choi, C. J. Kim, J. K. Lee, S. H. Kim, S. S. Kang and D.Khang, *ACS Nano.* 2013, **7**, 8484-8497.

Graphical abstract

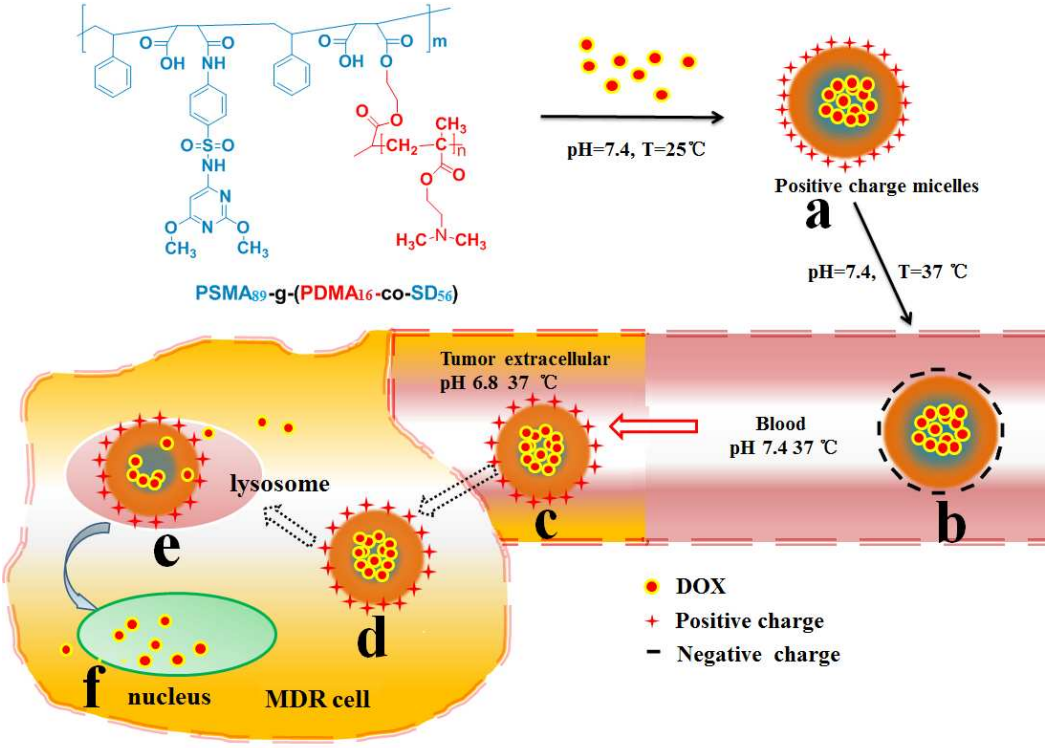

A novel thermo and pH dual-controlled charge reversal $PSMA_{89}$-g-P(DMA_{16}-co-SD_{56}) graft copolymer micelle was developed with effectively enhanced cellular uptake and overcoming multi-drug resistance in cancer cells.